Magphan Phantoms for MR for radiation therapy and quantitative imaging applications.

Smári

Sub-voxel geometric distortion measurements and critical image quality metrics engineered for ease of use in the clinical workflow.

The Phantom Laboratory manufactures high-precision phantoms coupled with Smári image analysis service and innovative custom solutions for the medical imaging and radiation therapy fields.

Click to see our latest phantoms and schedule a demo of our Smári image analysis service.

Robustness of sweeping-window arc therapy treatment sequences against intrafractional tumor motion

Jens Fleckenstein,[a] Jürgen Hesser, Frederik Wenz, and Frank Lohr
Department of Radiation Oncology, University Medical Center Mannheim, Heidelberg University, Theodor-Kutzer-Ufer 1-3, Mannheim 68167, Germany

(Received 29 April 2014; revised 30 January 2015; accepted for publication 5 February 2015; published 13 March 2015)

Purpose: Due to the potentially periodic collimator dynamic in volumetric modulated arc therapy (VMAT) dose deliveries with the sweeping-window arc therapy (SWAT) technique, additional manifestations of dosimetric deviations in the presence of intrafractional motion may occur. With a fast multileaf collimator (MLC), and a flattening filter free dose delivery, treatment times close to 60 s per fraction are clinical reality. For these treatment sequences, the human breathing period can be close to the collimator sweeping period. Compared to a random arrangement of the segments, this will cause a further degradation of the dose homogeneity.

Methods: Fifty VMAT sequences of potentially moving target volumes were delivered on a two dimensional ionization chamber array. In order to detect interplay effects along all three coordinate axes, time resolved measurements were performed twice—with the detector aligned in vertical (V) or horizontal (H) orientation. All dose matrices were then moved within a simulation software by a time-dependent motion vector. The minimum relative equivalent uniform dose $\mathrm{EUD}_{r,m}$ for all breathing starting phases was determined for each amplitude and period. Furthermore, an estimation of periods with minimum EUD was performed. Additionally, LINAC logfiles were recorded during plan delivery. The MLC, jaw, gantry angle, and monitor unit settings were continuously saved and used to calculate the correlation coefficient between the target motion and the dose weighed collimator motion component for each direction (CC, LR, AP) separately.

Results: The resulting $\mathrm{EUD}_{r,m}$ were $\mathrm{EUD}_{r,m}(\mathrm{CC}_V) = (98.3 \pm 0.6)\%$, $\mathrm{EUD}_{r,m}(\mathrm{CC}_H) = (98.6 \pm 0.5)\%$, $\mathrm{EUD}_{r,m}(\mathrm{AP}_V) = (97.7 \pm 0.9)\%$, and $\mathrm{EUD}_{r,m}(\mathrm{LR}_H) = (97.8 \pm 0.9)\%$. The overall minimum relative EUD observed for 360° arc midventilation treatments was 94.6%. The treatment plan with the shortest period and a minimum relative EUD of less than 97% was found at $T = 6.1$ s. For a partial 120° arc, an $\mathrm{EUD}_{r,m} = 92.0\%$ was found. In all cases, a correlation coefficient above 0.5 corresponded to a minimum in EUD.

Conclusions: With the advent of fast VMAT delivery techniques, nonrobust treatment sequences for human breathing patterns can be generated. These sequences are characterized by a large correlation coefficient between a target motion component and the corresponding collimator dynamic. By iteratively decreasing the maximum allowed dose rate, a low correlation coefficient and consequentially a robust treatment sequence are ensured. [http://dx.doi.org/10.1118/1.4914166]

Key words: VMAT, robust planning, interplay effects, organ motion, time resolved dosimetry

1. INTRODUCTION

Delivering dose to a moving target can potentially degrade the dose homogeneity in the target volume.[1,2] Various strategies to minimize the relative motion between the treatment beam and the target volume have been described for volumetric modulated arc therapy (VMAT):[3] The first approach is to treat the target volume in a static situation by using either respiratory gated radiation therapy[4] or active breath-hold techniques.[5,6] Since these techniques make use of only certain breathing phases, the treatment time is typically increased. The second approach is to perform a real-time adaptation of the multileaf collimator (MLC) aperture depending on the position of the target volume in beams-eye-view, known as dynamic multileaf collimator (dMLC) tracking.[7–9] While this approach has great potential to assure a fast and accurate treatment delivery, real-time information of the target position may not be available with sufficient accuracy. If neither gating nor tracking can be applied, treatments have to be performed in free breathing. For these cases, the resulting dosimetric effects have been theoretically predicted[10–13] and validated in experiments[14–18] and simulations.[19–23] Two manifestations of dosimetric errors have to be considered: dose blurring and interplay effects. A dose delivery with a static MLC while the target is moving results in a blurred (smeared out) dose distribution. A degradation of the resulting dose distribution in the target volume occurs adjacent to the gradients of the static dose distribution by the extent of the motion amplitude. In dose blurring, the expectation value of the dose in every voxel can be estimated by a convolution

of the dose distribution without motion and the probability density function (pdf) of the target motion. Nonrigid organ motion[24] and the changes in radiological depth due to target motion are not considered in this model (static dose cloud approximation[12]). According to the central limit theorem, every pdf converges to a Gaussian distribution if a sufficient number of fractions are delivered. Treatment planning in the presence of a blurred dose distribution is presented in AAPM report 91.[25] The planning target volume (PTV) is obtained by enlarging the clinical target volume (CTV) with an appropriate CTV–PTV margin.[26]

For a dynamic dose delivery, interplay or interference effects between the linear accelerator's (LINAC's) MLC and the target motion may be present. In contrast to a pure amplitude determined dose blurring, dosimetric errors can occur at all segment dose gradients within the target volume. Therefore, the pdf of a voxel no longer equals the pdf of the entire motion pattern. It has to be modified to only include the time intervals where a beam is actually contributing to the dose in the voxel. The structure of the temporo-spatial delivery pattern will have the highest impact when only a small number of fractions are delivered in combination with a fast, highly modulated treatment sequence. For these delivery types, a convergence of the voxel pdf to a Gaussian distribution may not be warranted.

Sweeping-window arc therapy (SWAT) relies on a change of the motion direction of the individual MLC leaves after a constant degree of gantry angle Θ (increment factor $\Delta\Theta$). VMAT dose deliveries with the SWAT technique[27] are therefore characterized by a potentially periodic motion of the collimator.[28] This feature allows, on the one hand, for a good starting condition during the treatment plan optimization and, on the other hand, it minimizes the amount of MLC leaf travel. This reduces the treatment time even further, compared to conventional VMAT. In SWAT, different collimator angles may be used. While Cameron[27] used 90° collimator angle and therefore an MLC leaf motion parallel to the axis of gantry rotation, Ulrich *et al.*[29] used 0° and Otto[3] 45° collimator angle. Intensity modulation is predominantly performed through dose rate and leaf speed variation,[3] which allows for a close to constant angular gantry rotation velocity.

Since in VMAT typically one arc is used, the phase relation cannot change on a beam-to-beam basis, as it is the case in step-and-shoot or dMLC IMRT treatments. With a fast MLC, and a flattening filter free (FFF) dose delivery, treatment times close to 60 s per fraction are clinical reality,[30] even for hypofractionated treatments with more than 5 Gy fraction dose. Since these treatment times contain only few breathing cycles, an averaging of the breathing pattern gets less likely and the human breathing period may get close to the collimator sweeping period. In analogy to the phenomenon of interference of temporally coherent waves, this may cause additional dosimetric deviations.

These facts require a further analysis of dosimetric robustness beyond the observations presented for IMRT.[11,12,17] To evaluate motion induced dosimetric artifacts specific to SWAT, three aspects shall be addressed: First, a method to quantify dosimetric artifacts in measured dose distributions in the presence of motion is presented; second, a theoretical prediction of breathing periods with minimum dose coverage is made; and third, a sensitive parameter that can be used to mitigate dosimetric deviations due to intrafractional target motion is identified and applied.

2. METHODS AND MATERIALS

2.A. Patient and treatment sequence collective

An Elekta (Stockholm, Sweden) Synergy LINAC with MLCi2 collimator and an Elekta VersaHD LINAC with Agility MLC were used for treatment sequence delivery. Treatment plans were generated with the Monaco 3.2/3.3 (Elekta) treatment planning system. Fifty different treatment plans for 13 different patients with lesions in lung (8), liver (2), stomach (1) or esophagus (2) were evaluated. Eight plans were generated using an MLCi2 collimator (fraction dose $D_{fx} = 2$ Gy), 28 plans were generated with an Agility collimator ($D_{fx} = 1.8$–3 Gy), and 14 plans were planned for a VersaHD LINAC for hypofractionated flattening filter free treatments ($D_{fx} = 5$–12 Gy). All treatment deliveries were performed with one 360° VMAT arc and increment factors $\Delta\Theta$ between 10° and 40°. The collimator angle was set to 0°, what resulted in a MLC leaf motion perpendicular to the axis of gantry rotation. Treatment volumes ranged from 12 to 2273 cm^3.

2.B. Estimation of the dose distribution in the presence of motion

All treatment sequences were delivered on a table-mounted, two dimensional ionization chamber array (Matrixx Evolution, IBA, Schwarzenbruck, Germany) inside a water equivalent phantom (Multicube Lite, IBA). The dose was recorded with a sampling time of $\Delta t = 100$ ms and stored in separate matrices. To be able to detect interplay effects along the three coordinate axes, all treatment sequences were delivered on the detector, aligned once in vertical and once in horizontal direction. A purpose written MATLAB® (Natick, MA) based script package was developed to evaluate the dose distribution in the presence of target motion. First, every matrix of the two dimensional measured static dose grid is interpolated to 2 mm spatial resolution. As shown in Fig. 1, the individual dose planes are then moved in either craniocaudal (CC), left–right (LR) or anterior–posterior (AP) direction. The nonzero component x_t of the target motion vector depends on the time after the start of the delivery t. It is determined according to Lujan *et al.*,[10]

$$x_t(A,T,\phi,t) = -\frac{A}{2} + A \times \cos^{2k}\left(\frac{\pi \cdot t}{T} + \phi\right), \quad (1)$$

where A is the peak-to-peak amplitude, T the breathing period, and ϕ the starting phase with respect to the treatment delivery start. The asymmetry factor k is in the following set to $k = 1$. The amplitude offset $-A/2$ in Eq. (1) mimics a dose delivery around midventilation phase. Finally, a summation of all time dependent dose matrices yields the cumulative

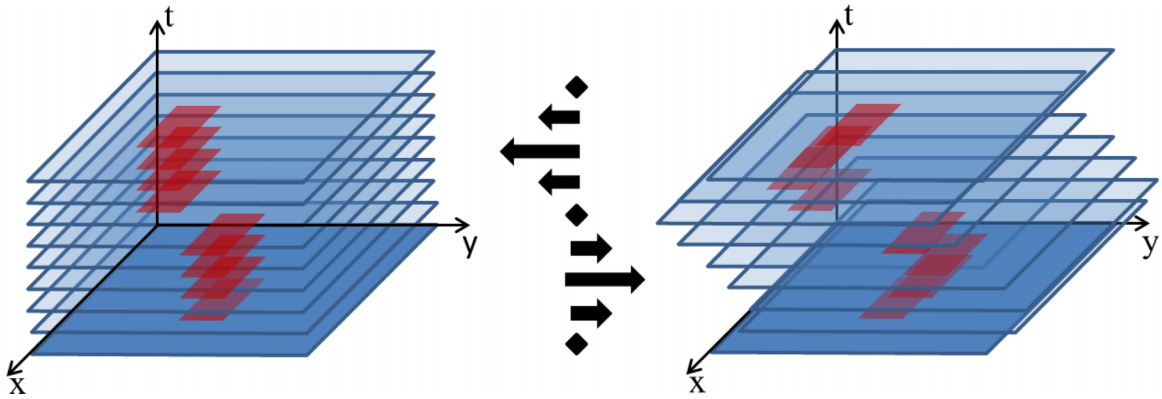

FIG. 1. Simulation of the dose distribution in the presence of motion. Individual time dependent dose distributions without target motion (left) and modified by a sine target motion (right) are shown. The rectangles in the central region represent nonzero dose levels while the rest equals zero dose.

dose distribution in the presence of motion. This procedure is performed for all 2.13×10^5 permutations of the following parameter sets: $A_{\text{sim}} = \{0.5\,\text{cm}, 1.0\,\text{cm}, 2.0\,\text{cm}\}$, $T_{\text{sim}} = \{1.0\,\text{s}, 1.1\,\text{s}, 1.2\,\text{s}, \ldots, 25.0\,\text{s}\}$, $\phi_{\text{sim}} = \{0°, 2.5°, 5°, \ldots, 177.5°\}$ and the four different target motion and detector orientation combinations: CC_H and LR_H for horizontal detector alignment as well as CC_V and AP_V for a vertical detector alignment. In a second step, the generated cumulative dose distributions are used to obtain the generalized equivalent uniform dose EUD (Refs. 31 and 32) as a function of motion amplitude, breathing period, and starting phase

$$\text{EUD}(A,T,\phi) = \left(\frac{1}{N}\sum_{l}^{N} D_l^a(A,T,\phi)\right)^{1/a}. \tag{2}$$

The EUD is calculated with $a = -25$ for all N dose pixels D_l with more than 70% of the maximum dose of the static dose distribution. The threshold dose value is motivated by the following consideration: For measurements in a phantom, the PTV structure is not available. Therefore, the maximum dose serves as a reference value. The dose within the target should be within 95%–107% of the prescription dose.[33] Additionally, the dose distribution in the phantom does not ideally resemble the dose distribution in the patient which can result in a further target dose inhomogeneity. Since in the patient the 95% isodose line should cover the PTV outline, a threshold value lower than 88% of the maximum dose, but still within the high dose gradient area, should be chosen to assure that all relevant voxels are being considered.

The factor a in Eq. (2) allows for an explicit selection of the degree of the minimum dose component (for $a = -\infty$) or the mean dose component (for $a = 1$). With the choice of $a = -25$, a result close to the minimum ROI dose but still sufficient dependency on the size of the underdosed volume is provided.

The minimum relative equivalent uniform dose $\text{EUD}_{r,m}$ is obtained by the ratio of the EUD of the dose slice if motion was present EUD_{dyn} and the EUD in the static case EUD_{stat}

$$\text{EUD}_{r,m}(A,T) = \frac{\min_{\phi\in\phi_{\text{sim}}}\{\text{EUD}_{\text{dyn}}(A,T,\phi)\}}{\text{EUD}_{\text{stat}}}. \tag{3}$$

The $\text{EUD}_{r,m}$ is obtained over all breathing starting phases. Phase averaged, the relative EUD equates the EUD of a pure dose blurring case, i.e., without consideration of the temporal substructure. The static case typically shows a nonuniform distribution in the target volume. Therefore, to be sensitive to motion-induced effects, the ratio of dynamic over static dose distribution was considered.

2.C. Estimation of periods with a minimum $\text{EUD}_{r,m}$

For motion in CC-direction, the jaws, which do not follow a sweeping window pattern, are the beam limiting devices. Motion in LR-direction was reported[34–36] to be generally less pronounced than motion in AP-direction. Therefore, for a collimator angle of 0°, target motion in AP-direction is most likely prone to SWAT-specific dosimetric errors and will be considered in this section.

In the presented model, dosimetric deviations resulting from target motion parallel to the central beam axis are neglected, and solely dose gradients along the beam penumbra are considered. This assumption is motivated by the fact that for a 6 MV beam with flattening filter and a $(5\times5)\,\text{cm}^2$ square field, the dose gradient along the central axis at 10 cm depth is $\text{d}D/\text{d}x_{\text{pdd}} = -3\%/\text{cm}$ of the maximum dose while the mean gradient between the 20% and the 80% penumbra dose at the same depth is $\text{d}D/\text{d}x_{\text{CL}} = \pm61\%/\text{cm}$ of the maximum dose.

To model a SWAT beam delivery, a treatment sequence with a sweeping collimator gap that performs s sweeps with an amplitude A_c and period t_{tot}/s, while the gantry performs one 360° considered. The dynamic of the resulting dose gradient areas is depending on two quantities: the current gantry angle and the position of the collimator gap. The impact of the gantry angle on the orientation of the penumbra with respect to the AP-direction of target motion can be described by a sine function of the current gantry angle, whereas the periodic collimator motion is modeled by another sine function. This yields an AP-component of the penumbra dynamic x_p of

$$x_p(t) = \underbrace{A_c \sin\left(\frac{2\pi}{t_{\text{tot}}/s}t\right)}_{\text{collimator component}} \times \underbrace{\sin\left(\frac{2\pi}{t_{\text{tot}}}t\right)}_{\text{gantry component}}. \tag{4}$$

The number of sweeps s is a function of the increment factor $\Delta\Theta$: $s = 360°/(2\cdot\Delta\Theta)$ defined during treatment planning. As a first order approximation for periodic breathing patterns, the target AP-motion can be assumed to perform a periodic motion. For $k = 1$, a constant amplitude A, and $\varphi = 2\phi + \pi/2$, Eq. (1) can be rearranged to

$$x_t(T,\varphi,t) = \frac{A}{2}\sin\left(\frac{2\pi}{T}t + \varphi\right). \tag{5}$$

In this model, the angular frequency $\omega_t = 2\pi/T$ corresponds to the dominant amplitude square component of any Fourier transformed irregular motion pattern. It is assumed that in SWAT, the gantry angle changes with a constant angular velocity $\dot{\Theta} = 2\pi/t_{\text{tot}}$. Therefore, the gantry angle Θ_1 is reached at $t = 1/4\,t_{\text{tot}}$ and Θ_2 at $t = 3/4\,t_{\text{tot}}$.

In order to achieve a maximum dosimetric deviation in the target volume, the two functions x_p and x_t have to be both extremal at Θ_1 and Θ_2

$$\left.\frac{\partial x_p}{\partial t}\right|_{t=1/4\,t_{\text{tot}};\,3/4\,t_{\text{tot}}} = \left.\frac{\partial x_t}{\partial t}\right|_{t=1/4\,t_{\text{tot}};\,3/4\,t_{\text{tot}}} = 0 \tag{6}$$

and both either in-phase (+) or of opposite-phase (−) around points with extremal AP-components Θ_1 and Θ_2

$$\left.\operatorname{sgn}\left(\frac{\partial^2 x_p}{\partial t^2}\right)\right|_{t=1/4\,t_{\text{tot}};\,3/4\,t_{\text{tot}}} = \pm\left.\operatorname{sgn}\left(\frac{\partial^2 x_t}{\partial t^2}\right)\right|_{t=1/4\,t_{\text{tot}};\,3/4\,t_{\text{tot}}}. \tag{7}$$

In the opposite-phase case, the target voxels avoid the beam to a maximum degree. For a target volume that is larger than the motion amplitude, this results in an underdosed central target region and an overdosed peripheral target region along the motion direction as well as an increased dose deposit outside the target. In the in-phase scenario, the target voxels follow the MLC sweep. Therefore, they accumulate more dose in the central target region while a sufficient target coverage at peripheral target regions is not guaranteed.

Between Θ_1 and Θ_2 an integer number of breathing cycles can take place [$T = t_{\text{tot}}/(2b)$, $b \in \mathbb{N}$] without changing the resulting behavior. From the above conditions, it follows that s has to be a positive, odd integer number. Solving the resulting system of equations yields for the two free target motion parameters T and φ

$$T = \frac{1}{2(s+Z)}t_{\text{tot}}, \tag{8}$$

$$\varphi = \pi\left(\frac{s}{2} - Z + p\right), \tag{9}$$

with $Z \in \mathbb{Z}$ and $p = 0$ for the opposite-phase case and $p = 1$ for the in-phase case. Equation (8) implies that the periods of maximum in-phase behavior are identical to the periods of maximum opposite-phase behavior.

2.D. Analysis of correlated motion patterns in SWAT

During plan delivery, the gantry angle, the cumulative monitor unit, and the individual MLC and jaw positions were recorded in LINAC logfiles with a frequency of 4 Hz. The Pearson correlation coefficient $r(x_c,x_t)$ for the collimator position component x_c along a specific axis (AP, LR, CC) and the target motion x_t in the same direction for a discrete sequence can be determined with

$$r(x_c,x_t) = \frac{1}{n-1}\sum_{i=1}^{n}\left(\frac{x_{c,i}-\bar{x}_{c,\omega}}{\sigma_{x_{c,\omega}}}\right)\left(\frac{x_{t,i}-\bar{x}_t}{\sigma_{x_t}}\right), \tag{10}$$

where i from 1 to n are the individual discrete times. Parallel to the direction of MLC leaf motion, this calculation is performed for all MLC leaves j that are not behind the craniocaudal jaws. Perpendicular to the direction of MLC leaf motion, the jaw positions are taken. The maximum correlation coefficient $r_{\max}(A,T)$ of all relevant leaves or jaws j_{rel} and of all starting phases ϕ_{rel} is obtained for each (A,T) combination

$$r_{\max}(A,T) = \max_{j\in j_{\text{rel}}}\left\{\max_{\phi\in\phi_{\text{rel}}}\left\{r(x_{c,j},x_t(A,T,\phi))\right\}\right\}. \tag{11}$$

Besides this purely geometrical consideration of the two dynamic patterns, a weight factor according to the dosimetric contribution of the segment has to be added. The relative weight is a product of the number of monitor units n_{MU} delivered in a time interval and the attenuation factor $r_{\text{att}}(\text{FS}_{\text{equ}},d)$. This factor is the relative dose of an equivalent square field of size FS_{equ} of the current segment at a depth d. d is the water equivalent distance traversed between patient or phantom surface and the beam isocenter. Therefore, the dose weighed mean can be expressed as

$$\bar{x}_{c,\omega} = \frac{\sum_{i=1}^{n}(n_{\text{MU}}r_{\text{att}})x_i}{\sum_{i=1}^{n}(n_{\text{MU}}r_{\text{att}})}, \tag{12}$$

and the weighed standard deviation is

$$\sigma_{c,\omega} = \sqrt{\frac{\sum_{i=1}^{n}(n_{\text{MU}}r_{\text{att}})(x_i-\bar{x}_{c,\omega})}{\sum_{i=1}^{n}(n_{\text{MU}}r_{\text{att}})}}. \tag{13}$$

3. RESULTS

Figure 2 shows an analysis of two representative treatment sequences. In the upper row, the minimum relative EUD as a function of the applied breathing period for different peak-to-peak breathing amplitudes is displayed, while the lower row shows the corresponding correlation coefficients between a target motion with $A = 2$ cm and the collimator dynamic AP-component. In both cases, motion in AP-direction was applied with the detector array being positioned in vertical alignment. The figures in the left column were generated with a treatment sequence of a target volume in the central right lung and were delivered with an MLCi2 collimator ($t_{\text{tot}} = 197$ s, $\Delta\Theta = 20°$), while the figures in the right column represent a treatment sequence for a target volume in the distal left lung, delivered with an Agility MLC ($t_{\text{tot}} = 61$ s, $\Delta\Theta = 20°$). The black circles indicate the predicted $\text{EUD}_{r,m}$ period times according to Sec. 2.C for $Z \in \{-6,-5,\ldots,3\}$. The minima with the lowest $\text{EUD}_{r,m}$ were found for $Z = -5$ for both cases. In the presented cases, the deviations between predicted and measured periods were (0.01 ± 0.08) s and (-0.04 ± 0.25) s.

In order to avoid high correlation coefficients within the range of human breathing periods, the maximum allowed

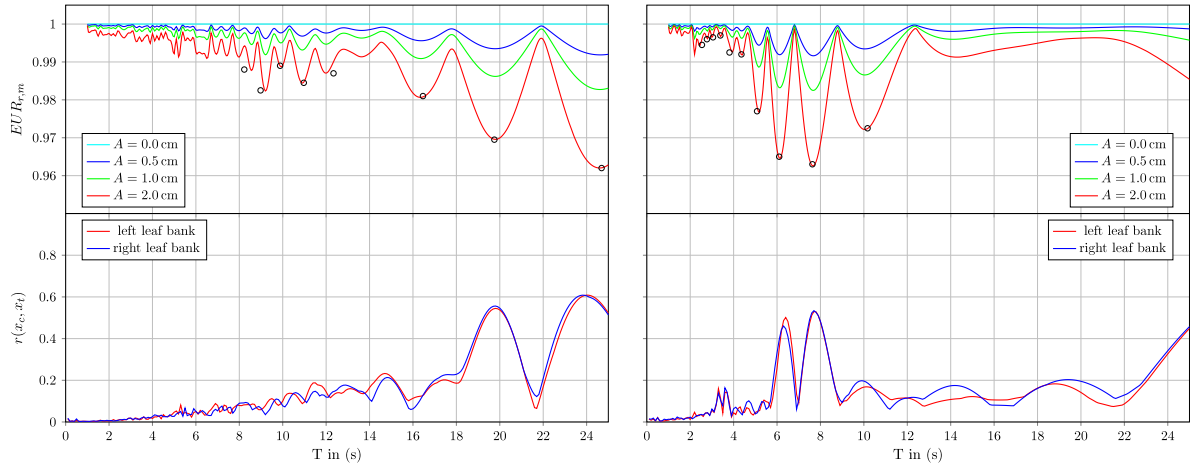

FIG. 2. Upper row: Relative maximum equivalent uniform dose $\mathrm{EUD}_{r,m}(A,T)$. Lower row: The corresponding maximum correlation coefficient $r(x_c, x_t)$. The presented treatment sequences were delivered with an MLCi2 collimator (left column), $\Delta\Theta = 20°$, $t_{\mathrm{tot}} = 197$ s and an Agility MLC (right column), $\Delta\Theta = 20°$, $t_{\mathrm{tot}} = 61$ s. The black circles indicate the predicted minima according to Sec. 2.C.

doserate $\dot{D}_{\max}$ of a treatment sequence can be reduced. The result of limiting $\dot{D}_{\max}$ on the periods with maximum cross correlation is presented in Fig. 3. The correlation coefficient between a target motion with different (A,T) settings and a collimator dynamic was obtained for three different $\dot{D}_{\max}$: 560, 400, and 270 monitor units per minute. The collimator dynamic of the left MLC leaf bank of the treatment sequence presented in Fig. 2 (right) was used for the determination of the correlation coefficients. For the presented treatment sequences, the resulting delivery times were 61, 76, and 109 s, respectively.

A dose delivery with a partial arc can lead to a further degradation of the dose homogeneity due to less dosimetric contributions from segments that move parallel to the motion direction. Therefore, the treatment sequence used in Fig. 2 on the right was limited to gantry angles between 40° and 160° with an increment of $\Delta\Theta = 20°$. The resulting analysis is shown in Fig. 4. A correlation coefficient of 0.94 resulted in a minimum $\mathrm{EUD}_{r,m}$ of 92.0%.

In Fig. 5, a measured dose distribution of the Agility MLC treatment sequence used in Fig. 2 without target motion is shown on the left. A target motion with $T = 6.1$ s, $A = 2$ cm, and $\phi = 90°$ $(Z = -4)$ was then applied. The corresponding dose differences to the static case are shown in Fig. 5 on the right. While the middle figure was generated with motion in CC-direction, the right figure was generated with motion in AP-direction.

The effect described in Sec. 2.C that in the opposite-phase case, dose from the central PTV regions gets deposited in peripheral regions due to an opposing motion of MLC leaves and patient breathing is demonstrated in the right figure.

The dose distributions represented the minimum $\mathrm{EUD}_{r,m}$ of this treatment sequence.

The $\mathrm{EUD}_{r,m}$ was determined for all treatment sequences and the four different motion scenarios. A histogram of the resulting $\mathrm{EUD}_{r,m}$ distribution of all simulated cases was

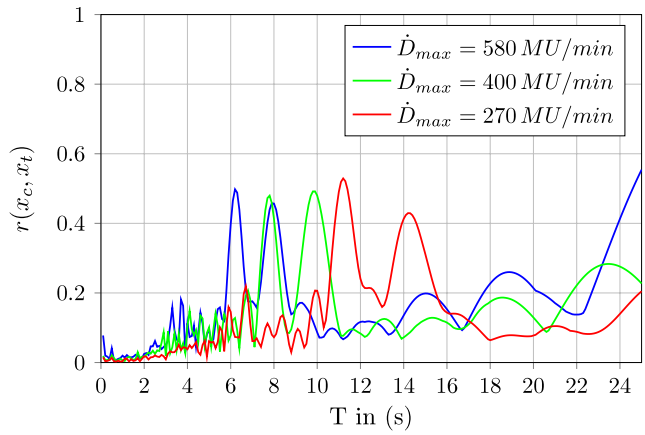

FIG. 3. Correlation coefficients for different maximum dose rates $\dot{D}_{\max}$. The collimator dynamic of the left MLC leaf bank of the treatment sequence presented in Fig. 2 (right) was used.

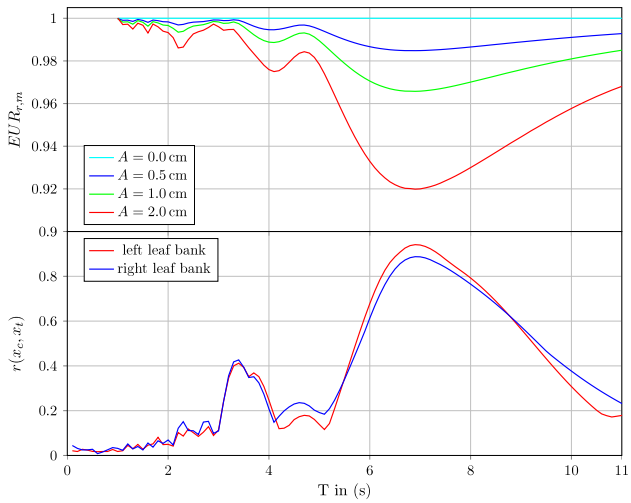

FIG. 4. Treatment sequence with a partial arc from 40° to 160° gantry angle. Upper row: Relative maximum equivalent uniform dose $\mathrm{EUD}_{r,m}(A,T)$. Lower row: Maximum correlation coefficient $r(x_c, x_t)$.

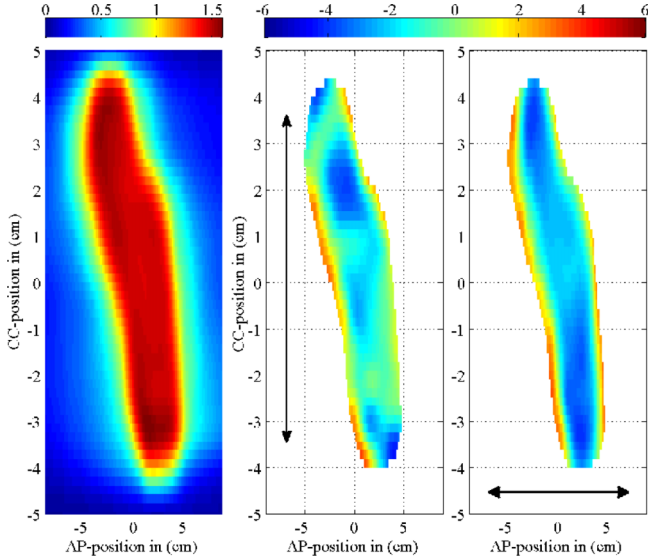

FIG. 5. Left: Measured dose distribution in (Gy) without target motion. Middle and right: Corresponding dose difference maps in (%) of the static case when a target motion with $T = 6.1$ s, $A = 2$ cm, and $\phi = 90°$ was applied. Black arrows indicate the direction of target motion.

created with an $\mathrm{EUD}_{r,m}$ bin width of 1%. This distribution is shown in Fig. 6.

The mean $\mathrm{EUD}_{r,m}$ were

- $\mathrm{EUD}_{r,m}(\mathrm{CC}_V) = (98.3 \pm 0.6)\%$,
- $\mathrm{EUD}_{r,m}(\mathrm{CC}_H) = (98.6 \pm 0.5)\%$,
- $\mathrm{EUD}_{r,m}(\mathrm{AP}_V) = (97.7 \pm 0.9)\%$, and
- $\mathrm{EUD}_{r,m}(\mathrm{LR}_H) = (97.8 \pm 0.9)\%$.

On average, the $\mathrm{EUD}_{r,m}$ for the target motion directions parallel to the MLC leaf motion direction was 0.7% lower when compared to a target motion perpendicular to the MLC leaf motion direction.

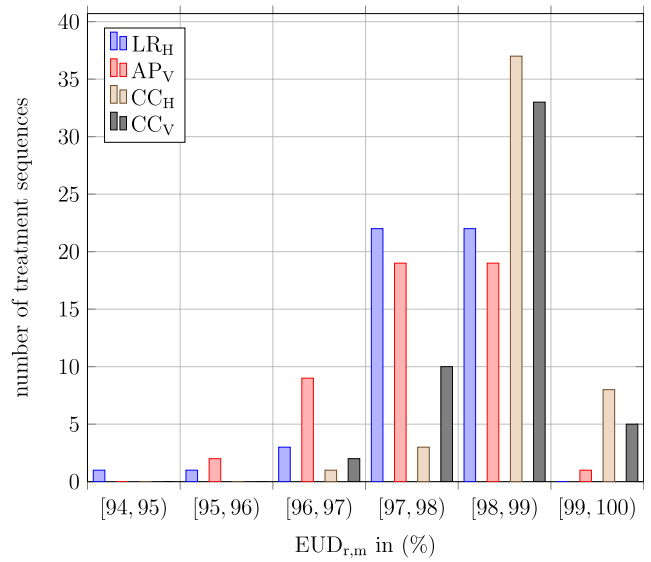

FIG. 6. Distribution of the minimum relative $\mathrm{EUD}_{r,m}$ values of all treatment sequences and the different motion directions.

TABLE I. Dependency of the number of sweeps on the minimum relative EUD.

$\Delta\Theta$ in deg	10	20	25	30	40
Number of sweeps	18.0	9.0	7.2	6.0	4.5
Number of sequences	3	18	3	12	4
$\overline{\mathrm{EUD}_{r,m}(\mathrm{AP}_V)}$ in (%)	97.7	97.0	97.9	98.1	97.5
$\sigma\left[\mathrm{EUD}_{r,m}(\mathrm{AP}_V)\right]$ in (%)	0.9	0.8	0.8	0.6	0.7

Table I shows the dependency of the applied number of sweeps on the $\mathrm{EUD}_{r,m}(\mathrm{AP}_V)$. Solely, treatment sequences of target volumes larger than 50 cm^3 were considered to ensure a pronounced sweep behavior. In agreement with the model presented in Sec. 2.C for 9 sweeps, the $\mathrm{EUD}_{r,m}(\mathrm{AP}_V)$ had the lowest mean value.

4. DISCUSSION

4.A. Suitability of the evaluation method

Various methods to evaluate the effect of target motion on the resulting dose distribution in IMRT and VMAT, such as Monte Carlo simulations[19] or measurements in suitable phantoms[14,16,18] with representative parameter settings have been performed. However, in SWAT, an appropriate selection of the parameters (A,T,Φ) is crucial for an accurate estimation of the worst possible treatment sequence. As shown in Fig. 2, the treatment plan robustness varied for different breathing periods. Increasing the target motion amplitude on the other hand showed a similar behavior over the entire period range.

Mean and standard deviations, as well as gamma analysis,[8] as measures for dosimetric errors are insensitive if the deviations affect only a small volume. If one considers exclusively minimum doses on the other hand the size of the underdosed volume is not taken into account. DVH based methods are either multidimensional[37] or use volumetric and dosimetric scalar quantities, such as V_{50} (%) or D_{95} (Gy), to evaluate the data. This kind of evaluation is typically being performed[38] for several dose or volume levels. In order to be able to observe the explicit dependence of the breathing period and amplitude on the treatment sequence robustness, the scalar $\mathrm{EUD}_{r,m}$ serves as an appropriate measure.

The Pearson correlation coefficient as presented in Eq. (11) is a measure of a linear correlation between the target and collimator motion. Nonlinear behavior will therefore lead to a reduced maximum correlation coefficient. However, if a random-like segment order was present, the correlation coefficient was close to 0 and a relatively low correlation coefficient threshold of 0.5 was sufficient to detect minima in $\mathrm{EUD}_{r,m}$ for all observed cases.

The use of a solid water phantom as a substitute for lung tissue will affect the dosimetric outcome. Therefore, the relative minimum EUD serves in this context more as a relative measure to indicate nonrobust frequencies than an absolute measure for the actual target EUD. The same applies for the choice of the parameter a in Eq. (2). Furthermore, in this study, solely the dosimetric consequences of a moving

target on the target volume were considered. In a realistic patient scenario, a nonrigid organs at risk (OAR) deformation will additionally affect the OAR doses, as well.

4.B. Dosimetric deviations in SWAT

A minimum in the $EUD_{r,m}$ results from a high correlation coefficient of the delivery pattern parallel to the target motion. If an extremal collimator elongation is opposed by an elongation in the same direction, an integer number of collimator sweeps between the two opposing beams will result in another minimum in $EUD_{r,m}$. It was shown in Fig. 5 that the manifestation of interplay effects changes in SWAT from spotlike artifacts, as presented in Fig. 5 (middle) or by Bortfeld *et al.*[11,12] for IMRT, to widespread underdosed areas as presented in Fig. 5 (right). Since all treatment plans were generated with 0° collimator angle, the sweeping windows moved parallel to the direction of gantry motion and caused dose deviations for target motion perpendicular to the gantry rotation axis to be on average 0.7% higher than the deviations resulting from motion parallel to the gantry rotation axis. The presented approach focuses on dose homogeneity in the PTV, whereas the CTV is the relevant structure that will affect the treatment efficiency. For standard IMRT, the location of the underdosed volume within the PTV remains unknown with this approach. In the case of SWAT, a nonrobust breathing period will, provided an unfortunate starting phase is chosen, generate an underdosed area in the central region of the PTV [Fig. 5 (right)]. As CTV–PTV margins are usually chosen symmetrically around the CTV, (Ref. 25) the underdosage will occur in the CTV.

4.C. Robust treatment planning in SWAT

While the motion amplitude is used to determine the PTV margin during treatment planning,[33] the breathing period is typically not considered. One option to minimize interplay effects in SWAT is to increase the increment parameter to reduce the number of sweeps. The human breathing is typically between 9 and 23 breathing cycles per minute.[36]

Provided that the rotational velocity of the gantry does not exceed $\dot{\Theta} \leq 2\pi/60\,\mathrm{s}$ in combination with the results from Table I, care should be taken if choosing an increment factor of $\Delta\Theta = 20°$.

Using multiple arcs with different increment factors or collimator angles during treatment delivery will further desynchronize the delivery pattern. For treatment plans, in which the treatment volume is located laterally, most of the dose will originate from a subarc around 90° or 270° gantry angle, where the motion component in AP-direction is maximal. These cases have to be considered with special care, since an averaging of opposing beamlets and dosimetric contributions from beamlets, where the target moves parallel to the central axis of the beam, will not be present.

For standard IMRT, Jiang *et al.*[14] recommend to use a low dose rate when treating a moving tumor without any motion mitigation techniques. The presented approach can be considered as a quantitative method to obtain the fastest robust treatment sequence for VMAT with a sweeping window collimator dynamic. An iterative decrease of the maximum dose rate can be used to alter the temporal behavior of the delivery pattern x_p. For x_t, a realistic target trajectory can be obtained from 4D-CT data. Due to interfractional changes in the breathing pattern, it is recommended to test against additional realistic breathing patterns. This procedure provides the possibility to produce robust sequences without having to reoptimize the treatment sequence. As the presented minima in $EUD_{r,m}$ are typically temporally local, a small decrease in treatment time will suffice to move out of a minimum. Chin *et al.*[9] adjusted the increment factors to match the patient breathing, obtained from 4D-CT data. While this is the optimum method if the patient breathing trajectory is known, the method presented in this work does not rely on an exact knowledge of the target dynamic during treatment delivery. Although it does not warrant a reduction of safety margins, it assures a fast convergence to a pure dose blurring situation.

5. CONCLUSION

With the advent of fast delivery techniques less robust treatment plans within the human breathing range can be generated. In SWAT, the correlation coefficient between the collimator pattern and realistic motion trajectories serves as an estimate for the plan robustness. By iteratively decreasing the maximum dose rate, a robust treatment sequence can be warranted. No degradation of the relative minimum EUD above 8.0% compared to the static case was found.

ACKNOWLEDGMENT

This work was supported by an Elekta research grant held by F.W. and F.L.

[a]Electronic mail: Jens.Fleckenstein@medma.uni-heidelberg.de

[1]S. Webb, "Motion effects in (intensity modulated) radiation therapy: A review," Phys. Med. Biol. **51**, R403–R425 (2006).
[2]S. S. Korreman, "Motion in radiotherapy: Photon therapy," Phys. Med. Biol. **57**, R161–R191 (2012).
[3]K. Otto, "Volumetric modulated arc therapy: IMRT in a single gantry arc," Med. Phys. **35**, 310–317 (2008).
[4]G. Nicolini, E. Vanetti, A. Clivio, A. Fogliata, and L. Cozzi, "Pre-clinical evaluation of respiratory-gated delivery of volumetric modulated arc therapy with RapidArc," Phys. Med. Biol. **55**, N347–N357 (2010).
[5]H. A. McNair, J. Brock, J. R. N. Symonds-Tayler, S. Ashley, S. Eagle, P. M. Evans, A. Kavanagh, N. Panakis, and M. Brada, "Feasibility of the use of the active breathing coordinator (ABC) in patients receiving radical radiotherapy for non-small cell lung cancer (NSCLC)," Radiother. Oncol. **93**, 424–429 (2009).
[6]J. Boda-Heggemann, S. Mai, J. Fleckenstein, K. Siebenlist, A. Simeonova, M. Ehmann, V. Steil, F. Wenz, F. Lohr, and F. Stieler, "Flattening-filter-free intensity modulated breath-hold image-guided SABR (Stereotactic ABlative Radiotherapy) can be applied in a 15-min treatment slot," Radiother. Oncol. **109**, 505–509 (2013).
[7]G. A. Davies, G. Poludniowski, and S. Webb, "MLC tracking for Elekta VMAT: A modelling study," Phys. Med. Biol. **56**, 7541–7554 (2011).
[8]T. Ravkilde, P. J. Keall, C. Grau, M. Høyer, and P. R. Poulsen, "Time-resolved dose distributions to moving targets during volumetric modulated

arc therapy with and without dynamic MLC tracking," Med. Phys. **40**, 111723 (8pp.) (2013).
[9]E. Chin, S. K. Loewen, A. Nichol, and K. Otto, "4D VMAT, gated VMAT, and 3D VMAT for stereotactic body radiation therapy in lung," Phys. Med. Biol. **58**, 749–770 (2013).
[10]A. E. Lujan, E. W. Larsen, J. M. Balter, and R. K. Ten Haken, "A method for incorporating organ motion due to breathing into 3D dose calculations," Med. Phys. **26**, 715–720 (1999).
[11]T. Bortfeld, K. Jokivarsi, M. Goitein, J. Kung, and S. B. Jiang, "Effects of intra-fraction motion on IMRT dose delivery: Statistical analysis and simulation," Phys. Med. Biol. **47**, 2203–2220 (2002).
[12]T. Bortfeld, S. B. Jiang, and E. Rietzel, "Effects of motion on the total dose distribution," Semin. Radiat. Oncol. **14**, 41–51 (2004).
[13]M. Engelsman, E. M. F. Damen, K. De Jaeger, K. M. van Ingen, and B. J. Mijnheer, "The effect of breathing and set-up errors on the cumulative dose to a lung tumor," Radiother. Oncol. **60**, 95–105 (2001).
[14]S. B. Jiang, C. Pope, K. M. Al Jarrah, J. H. Kung, T. Bortfeld, and G. T. Y. Chen, "An experimental investigation on intra-fractional organ motion effects in lung IMRT treatments," Phys. Med. Biol. **48**, 1773–1784 (2003).
[15]M. Schaefer, C. Münter, M. W. Thilmann, F. Sterzing, P. Haering, S. E. Combs, and J. Debus, "Influence of intra-fractional breathing movement in step-and-shoot IMRT," Phys. Med. Biol. **49**, N175–N179 (2004).
[16]C. Vrančić, A. Trofimov, T. C. Y. Chan, G. C. Sharp, and T. Bortfeld, "Experimental evaluation of a robust optimization method for IMRT of moving targets," Phys. Med. Biol. **54**, 2901–2914 (2009).
[17]E. D. Ehler, B. E. Nelms, and W. A. Tomé, "On the dose to a moving target while employing different IMRT delivery mechanisms," Radiother. Oncol. **83**, 49–56 (2007).
[18]C. Stambaugh, B. E. Nelms, T. Dilling, C. Stevens, K. Latifi, G. Zhang, E. Moros, and V. Feygelman, "Experimentally studied dynamic dose interplay does not meaningfully affect target dose in VMAT SBRT lung treatments," Med. Phys. **40**, 091710 (8pp.) (2013).
[19]J. Seco, G. C. Sharp, Z. Wu, D. Gierga, F. Büttner, and H. Paganetti, "Dosimetric impact of motion in free-breathing and gated lung radiotherapy: A 4D Monte Carlo study of intrafraction and interfraction effects," Med. Phys. **35**, 356–366 (2008).
[20]J. Seco, D. Robertson, A. Trofimov, and H. Paganetti, "Breathing interplay effects during proton beam scanning: Simulation and statistical analysis," Phys. Med. Biol. **54**, N283–N294 (2009).
[21]M. Oliver, A. Gladwish, R. Staruch, J. Craig, S. Gaede, J. Chen, and E. Wong, "Experimental measurements and Monte Carlo simulations for dosimetric evaluations of intrafraction motion for gated and ungated intensity modulated arc therapy deliveries," Phys. Med. Biol. **53**, 6419–6436 (2008).
[22]Y. D. Mutaf, C. J. Scicutella, D. Michalski, K. Fallon, E. D. Brandner, G. Bednarz, and M. S. Huq, "A simulation study of irregular respiratory motion and its dosimetric impact on lung tumors," Phys. Med. Biol. **56**, 845–859 (2011).
[23]L. Court, M. Wagar, R. Berbeco, A. Reisner, B. Winey, D Schofield, D. Ionascu, A. M. Allen, R. Popple, and T. Lingos, "Evaluation of the interplay effect when using RapidArc to treat targets moving in the craniocaudal or right-left direction," Med. Phys. **37**, 4–11 (2010).
[24]J. G. Li and L. Xing, "Inverse planning incorporating organ motion," Med. Phys. **27**, 1573–1578 (2000).
[25]P. J. Keall, G. S. Mageras, J. M. Balter, R. S. Emery, K. M. Forster, S. B. Jiang, J. M. Kapatoes, D. A. Low, M. J. Murphy, B. R. Murray, C. R. Ramsey, M. B. van Herk, S. S. Vedam, J. W. Wong, and E. Yorke, "The management of respiratory motion in radiation oncology report of AAPM task group 76," Med. Phys. **33**, 3874–3900 (2006).
[26]M. van Herk, "Different styles of image-guided radiotherapy," Semin. Radiat. Oncol. **17**, 258–267 (2007).
[27]C. Cameron, "Sweeping-window arc therapy: An implementation of rotational IMRT with automatic beam-weight calculation," Phys. Med. Biol. **50**, 4317–4336 (2005).
[28]C. X. Yu, D. A. Jaffray, and J. W. Wong, "The effects of intra-fraction organ motion on the delivery of dynamic intensity modulation," Phys. Med. Biol. **43**, 91–104 (1998).
[29]S. Ulrich, S. Nill, and U. Oelfke, "Development of an optimization concept for arc-modulated cone beam therapy," Phys. Med. Biol. **21**, 4099–4119 (2007).
[30]D. Georg, T. Knöös, and B. McClean, "Current status and future perspective of flattening filter free photon beams," Med. Phys. **38**, 1280–1293 (2011).
[31]A. Nimierko, "Reporting and analyzing dose distributions: A concept of equivalent uniform dose," Med. Phys. **24**, 103–110 (1997).
[32]Q. Wu, R. Mohan, A. Nimierko, and R. Schmidt-Ulrich, "Optimization of intensity-modulated radiotherapy plans based on equivalent uniform dose," Int. J. Radiat. Oncol., Biol., Phys. **52**, 224–235 (2002).
[33]V. Gregoire, T. R. Mackie, W. De Neuve, M. Gospodarowicz, J. A. Purdy, M. van Herk, and A. Nimierko, "ICRU report 83: Presribing, recording and reporting photon-beam intensity-modulated radiation therapy (IMRT)," J. ICRU **10**, 1–106 (2010).
[34]R. George, S. S. Vedam, T. D. Chung, V. Ramakrishnan, and P. J. Keall, "The application of the sinusoidal model to lung cancer patient respiratory motion," Med. Phys. **32**, 2850–2861 (2005).
[35]Y. Seppenwoolde, H. Shirato, K. Kitamura, S. Shimizu, M. van Herk, J. V. Lebesque, and K. Miyasaka, "Precise and real-time measurement of 3D tumor motion in lung due to breathing and heartbeat, measured during radiotherapy," Int. J. Radiat. Oncol., Biol., Phys. **53**, 822–834 (2002).
[36]H. Shirato, A. Seppenwoolde, K. Kitamura, R. Onimura, and S. Shimizu, "Intrafractional tumor motion: Lung and liver," Semin. Radiat. Oncol. **14**, 10–18 (2004).
[37]M. Söhn, B. Sobotta, and M. Alber, "Dosimetric treatment course simulation based on a statistical model of deformable organ motion," Phys. Med. Biol. **57**, 3693–3709 (2012).
[38]Z. Hui, X. Zhang, G. Starkschall, Y. Li, R. Mohan, R. Komaki, J. D. Cox, and J. Y. Chang, "Effects of intrafractional motion and anatomic changes on proton therapy dose distributions in lung cancer," Int. J. Radiat. Oncol., Biol., Phys. **72**, 1385–1395 (2008).